PROCEEDINGS of the
23rd International Congress on Acoustics
9 to 13 September 2019 in Aachen, Germany

Adjoint-based sound reinforcement in the time domain

Lewin STEIN[(1)], Florian STRAUBE[(2)], Jörn SESTERHENN[(1)], Stefan WEINZIERL[(2)], Mathias LEMKE[(1)]

[(1)]Computational Fluid Dynamics Group at Technische Universität Berlin, Germany
[(2)]Audio Communication Group at Technische Universität Berlin, Germany

1 Jun 2019

Abstract
The determination of the electronic drive of line source arrays is an ill-posed inverse problem. The authors present an adjoint-based approach in the time domain as an alternative to the commonly used frequency-based methods. Therein, monopole sources in the EULER equations are optimized to reinforce a prescribed target sound field. In doing so, driving functions for the synthesis of the desired sound field, including a non-uniform base flow, can be determined.

Keywords: loudspeaker arrays, sound reinforcement, acoustic time-reversal, monopole sources

1 INTRODUCTION

Sound reproduction, sound reinforcement, and source identification methods are typically based on frequency domain approaches and restricted to the wave equation with a homogeneous background flow [1, 2, 3, 4]. In contrast, we suggest an adjoint-based solution of the EULER equations in the time domain for the following reasons: The EULER equations, as a generalized form of the wave equation, allow to consider inhomogeneous background flow and nonlinear sound effects. The adjoint-based approach (time-reversal) facilitates to simultaneously optimize all degrees of freedoms (control parameters), for example the speaker alignment, the signal amplitude and the phase over the entire frequency range of arbitrary line arrays. The computational cost of a conventional parameter study (only forward in time) increases linearly with the degree of freedom, while the computational costs of the adjoint approach do not increase with the number of optimized parameters, instead, they remain constant.

2 METHOD

For a better understanding of the results, a brief overview of the adjoint-based computational aero-acoustic (CAA) solver is given in the following. An introduction of the method with more details can be found in [5].

2.1 Basic idea of the adjoint approach

The adjoint equations can be derived in a continuous or discrete manner. Here, for the sake of simplicity, they are introduced in a discrete version as in [6]. A matrix-vector notation is used. The vector space is the full solution in space and time. For a complete discussion on the derivation, the reader is referred to [7, 8].

Adjoint equations arise by a so-called objective function J, which is defined by the product between a geometric weight g and the system state q.

$$J = g^{\mathrm{T}} q \tag{1}$$

The system state q corresponds to the solution of the governing system

$$A\,q = s \tag{2}$$

with A as governing operator and s as source terms on the right-hand side. To optimize J by means of s, the equation has to be solved for all s. In order to reduce the computational effort, the adjoint equation can be

used

$$A^{\mathrm{T}} q^* = g, \tag{3}$$

with the adjoint variable q^*. By

$$J = g^{\mathrm{T}} q = \left(A^{\mathrm{T}} q^*\right)^{\mathrm{T}} q = q^{*\mathrm{T}} A q = q^{*\mathrm{T}} s \tag{4}$$

an expression is found, which enables the computation of J without the need to solve the system for every discrete s at once. After calculating the adjoint equation, i.e. q^*, the objective J can be determined by a simple and computationally cheap scalar product (Eq. 4). Thus, the adjoint approach enables the efficient computation of J gradients with respect to s.

2.2 Incorporated CAA equations and optimization target

According to the intended application – the adjoint-based sound field generation in the time domain – the objective function J is defined in space and time as

$$J = \frac{1}{2} \iint \left(p' - p'_{\mathrm{target}}\right)^2 \sigma(x_i, t) \mathrm{d}\Omega. \tag{5}$$

The variable p'_{target} ($p = p_0 + p'$) denotes the desired sound field, resulting from quality characteristics for sound reinforcement tasks, such as a specific volume distribution or a smooth frequency response. The weight $\sigma(x_i, t)$ defines where and when the objective is evaluated. Optimal sound reinforcement is realized if J reaches a minimum.

The minimum is to be achieved under the constraint that the EULER equations

$$\partial_t \begin{pmatrix} \rho \\ \rho u_j \\ \frac{p}{\gamma - 1} \end{pmatrix} + \partial_{x_i} \begin{pmatrix} \rho u_i \\ \rho u_i u_j + p \delta_{ij} \\ \frac{u_i p \gamma}{\gamma - 1} \end{pmatrix} - u_i \partial_{x_i} \begin{pmatrix} 0 \\ 0 \\ p \end{pmatrix} = \begin{pmatrix} 0 \\ 0 \\ s \end{pmatrix} \tag{6}$$

abbreviated as $E(q)\, q = s$ are satisfied, with q as state vector and s as a source term. The general goal is to obtain a solution which matches $p'_{\mathrm{target}}(q)$ of Eq. 5 in an optimal sense by adapting the source term s, which can be interpreted as multiple loudspeakers.

In order to use the adjoint approach for optimizing s, it is necessary to linearize the objective function and the governing system (6). This results in

$$\delta J = \iint \underbrace{\left(q - q_{\mathrm{target}}\right) \sigma}_{=g} \delta q \mathrm{d}\Omega, \tag{7}$$

and

$$E_{\mathrm{lin}}(q_0) \delta q = \delta s \tag{8}$$

with a redefined weight $g = (q - q_{\mathrm{target}})\sigma$. Combining the linearized system and the objective in a Lagrangian manner by introducing the (adjoint) multiplier q^*, leads to

$$\begin{aligned} \delta J &= g^{\mathrm{T}} \delta q - q^{*\mathrm{T}} \underbrace{\left(E_{\mathrm{lin}}(q_0) \delta q - \delta s\right)}_{=0}, \\ &= q^{*\mathrm{T}} \delta s + \delta q^{\mathrm{T}} \left(g - E_{\mathrm{lin}}^{\mathrm{T}}(q_0) q^*\right). \end{aligned} \tag{9}$$

For the sake of simplicity, the integrals are not shown. The adjoint equations result in

$$g - E_{\mathrm{lin}}^{\mathrm{T}}(q_0) q^* = 0, \tag{10}$$

with q^* as adjoint state vector. The change of the objective function reads

$$\delta J = q^{*\mathrm{T}} \delta s, \tag{11}$$

similar to (4). Thus, the adjoint solution can be interpreted as a gradient of J with respect to the source term s

$$\nabla_s J = q^*. \tag{12}$$

A more detailed derivation of the adjoint approach is discussed in [5, 8, 9].

2.3 The adjoint CAA solver

The driving functions for given speaker positions are determined and optimized iteratively:

1. Initially, guess the loudspeaker source terms $s^0 = 0$.
2. Solve the governing EULER equations (6) with s^i. Here, the exponent $i = 0$ is the first iteration step.
3. Compare with the desired target solution and break if a suitable convergence criterion is reached.
4. Solve the adjoint EULER equations (10).
5. Compute the gradient $\nabla_s J$ using the adjoint solution.
6. Update the current forcing $s^{i+1} = s^i + \nabla_s J$.
7. Repeat, starting with 2.

The resulting optimal s is deconvolved with the considered primitive input signal defining p'_{target} and the loudspeaker properties (e.g. electronic filters) resulting in an optimal driving for every considered loudspeaker. The solutions shown in this work are the result of fifteen iteration steps.

Numerical specifications (parallelization, resolution, spatial derivative, time integration, filters, boundary conditions) of the adjoint CAA solver are listed in [5], i.e., originally in [7, 10].

3 TEST CASE

The three-dimensional test case studied here (Fig. 1) contains a line array with five monopoles speakers, i.e. spherical loudspeakers, which are aligned in an x_1-line at $x_1 = (0.4, 0.6, 0.8, 1.0, 1.2)\,\mathrm{m}$, and constant $x_2 = 0.8\,\mathrm{m}$ and $x_3 = 0.8\,\mathrm{m}$.

The audience, i.e., the mask σ (Eq. 5), is located symmetrically around the line array at a minimal distance of $0.175\,\mathrm{m}$ and a maximal distance of $0.4\,\mathrm{m}$. The physical domain is evaluated at an equidistant rectangular grid with a spacing of $dx = 1.6/197\,\mathrm{m}$ and with a temporal sampling rate of 48 kHz.

As homogeneous background medium air is approximated as an ideal gas with a speed of sound $c_0 = 343\,\mathrm{m/s}$, a density of $\rho_0 = 1.21\,\mathrm{kg/m^3}$, a pressure $p_0 = 101\,325\,\mathrm{Pa}$, an adiabatic index $\gamma = 1.4$ and a specific gas constant $R_s = 287$.

As a test signal for all monopole speakers, a sine sweep with an exponential frequency increase and a constant amplitude over time (see $\tilde{s}_{\mathrm{CAA}}$ in Fig. 2) is used. Below 1.3 kHz and above 2.7 kHz the sweep has a fade in and fade out period. At the end of the sweep, there is 1 ms silence (the last 48 time steps). Throughout this paper the frequency spectrum between 1.3 kHz and 2.7 kHz is evaluated. The initial transient is not discussed here. To study a practically relevant spatially inhomogeneous SPL distribution the relative amplitudes and phases between the signals differ among all speakers. With increasing x_1-position the signal amplitude decreases (cf. Fig. 1).

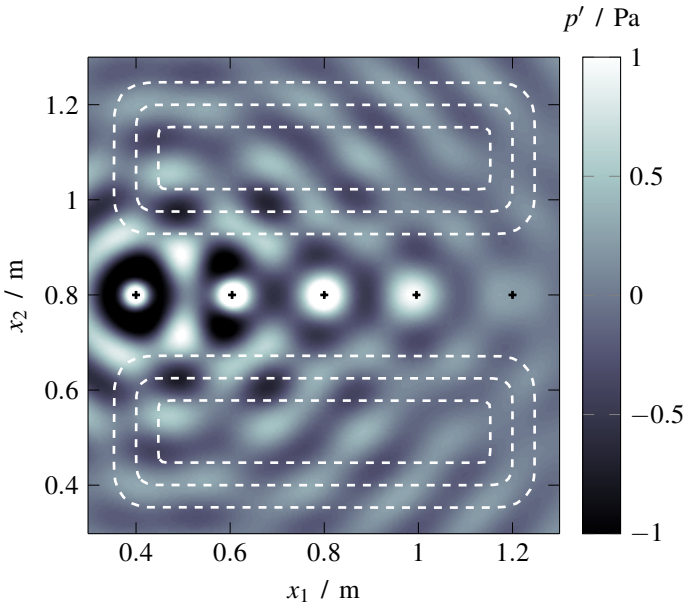

Figure 1. Sound field radiated by a line array with five monopole sources. A snapshot of the pressure reference field at a central x_1x_2-slice ($x_3 = 0.8\,\mathrm{m}$) is shown, where all speakers are located. Isolines of the objective weight function σ (Eq. 5) at values of 0.01, 0.5, and 0.99 are denoted by white, dashed lines.

4 RESULTS

As a reference solution, a complex-directivity point source (CDPS) model in the frequency domain is utilized [3, 4, 11]. The CDPS model provides, for a prescribed sine sweep $\tilde{s}_{\mathrm{CDPS}}$, the reference field p'_{target} (Eq. 5) for all spatial and temporal locations. With the reference field and the source locations as input, the CAA framework iteratively recalculates the amplitude and phase of the driving sine sweep s. By comparing s with the original signal $\tilde{s}_{\mathrm{CDPS}}$ the adjoint-based approach is validated. We verify to which extent the adjoint approach is able to identify the optimal excitation signals for a given sound field.

In this work, the signals are optimized for predefined fixed speaker alignment. However, in general, the adjoint approach is also capable to identify speaker locations [9].

4.1 Conversion and comparability of source terms with and without flow

To obtain comparable – physically equivalent – forms of source terms called $\tilde{s}_{\mathrm{CAA}}$ and $\tilde{s}_{\mathrm{CDPS}}$, s of Eq. 6 needs to be converted to $\tilde{s}_{\mathrm{CAA}}$: While $\tilde{s}$ denotes a source term of the wave equation (second time derivative), s is a source term of the pressure equation (first time derivative). $\tilde{s}_{\mathrm{CDPS}}$ of the CDPS model drives an ideal monopole speaker, i.e., a Dirac delta function. In contrast s of the CAA solver consists of an entire Gaussian distribution of monopoles, which taken all together approximate a single monopole speaker. A single Dirac delta source would create instabilities (Runge phenomenon), while its smoothed alternative representation as Gaussian distribution – applied here – is numerically more stable. We derive in the following a conversion rule between s and $\tilde{s}_{\mathrm{CAA}}$, which will be applied later to compare $\tilde{s}_{\mathrm{CAA}}$ and $\tilde{s}_{\mathrm{CDPS}}$ in their physically equivalent form.

The linearized momentum and energy equation of the EULER equations (Eq. 6) of the CAA solver (without flow) are

$$\begin{pmatrix} \rho_0 \partial_t u'_j \\ \frac{\partial_t p'}{\gamma - 1} \end{pmatrix} + \begin{pmatrix} \partial_{x_j} p' \\ \frac{\gamma p_0 \nabla u'}{\gamma - 1} \end{pmatrix} = \begin{pmatrix} 0 \\ s \end{pmatrix}. \tag{13}$$

The time derivative and the combination of both equations gives the wave equation

$$\partial_t^2 p' - c_0^2 \Delta p' = (\gamma - 1)\partial_t s(y,t)\,, \tag{14}$$

where $s(y,t)$ is the related force term. Since we assume an ideal gas, $c_0^2 = \gamma p_0/\rho_0$ holds.
The general solution of the inhomogeneous wave equation in free space is known as

$$p'(x,t) = \frac{\gamma - 1}{4\pi} \int_{\mathbb{R}^3} \frac{\partial_\tau s(y,\tau)}{|x-y|} dy\,, \tag{15}$$

with the delayed time $\tau = t - |x-y|/c_0$. As discussed before, to ensure numerical stability, the CAA solver uses an entire Gaussian shaped distribution of monopoles

$$s(y,t) = \frac{1}{\gamma - 1} \sum_m \mathrm{e}^{-(y_m - y_0)^2 \mu^{-2}} \delta(y_m - y) s_{\mathrm{CAA}}(t) \tag{16}$$

instead of a pure monopole source located at y_0. $s_{\mathrm{CAA}}(t)$ is the time signal, which is driving all individual monopoles of the Gaussian distribution. The monopole positions are numbered with the index m. The variance of the Gauss is set as $\mu = 2\Delta x$. Hence μ is eight times smaller than the shortest acoustic wavelength evaluated here (2.7 kHz).
Combining the latter equations provides

$$p'(x,t) = \sum_m \mathrm{e}^{-(y_m - y_0)^2 \mu^{-2}} \frac{\partial_\tau s_{\mathrm{CAA}}(\tau_m)}{4\pi r_m}\,, \tag{17}$$

being $\tau_m = t - r_m/c_0$ the delayed time due to the distance $r_m = |x - y_m|$ between the observer x and each monopole position y_m.
In case of a homogeneous background flow in x_1-direction with a Mach number M, the solution follows

$$p'(x,t) = \sum_m \mathrm{e}^{-(y_m - y_0)^2 \mu^{-2}} \left\{ \frac{c_0 M \cos(\theta_m)}{4\pi r_m^2 a_m^3} s_{\mathrm{CAA}}(\tau_m^+) + \frac{1 - M\cos(\theta_m)/a_m}{4\pi r_m (1-M^2) a_m} \partial_{\tau^+} s_{\mathrm{CAA}}(\tau_m^+) \right\}, \tag{18}$$

being $\tau_m^+ = t - r_m(a_m - M\cos\theta_m)/(1-M^2)/c_0$, $a_m^2 = 1 - M^2\sin^2(\theta_m)$, and $\cos(\theta_m) = (x_1 - y_{1m})/r_m$, see [12]. In case the mic is placed in the far-field downstream of the source with $\theta_m \cong 0$, this simplifies to

$$p'(x,t) = \sum_m \mathrm{e}^{-(y_m - y_0)^2 \mu^{-2}} \frac{\partial_{\tau^+} s_{\mathrm{CAA}}(\tau_m^+)}{4\pi r_m (1+M)}\,. \tag{19}$$

In contrast to Eq. 14, the CDPS model solves the wave equation

$$\partial_t^2 p' - c_0^2 \Delta p' = \delta(y_0 - y)\tilde{s}(t)\,, \tag{20}$$

with a different source type, denoted by the overlying tilde. Instead of a Gaussian monopole distribution, the CDPS model uses a single monopole at the center of the Gauss $\delta(y_0 - y)$. The CDPS model sets $\tilde{s}(t) = s_{\mathrm{CDPS}}$ directly equal to the test signal, i.e., the exponential sine sweep. Please note here the difference between the signals $\tilde{s}(t)$ of Eq. 20 and $s(t)$ of Eq. 14, especially the time derivative. The far-field solution of Eq. 20 is

$$p'(x,t) = \frac{\tilde{s}(\tau_0^+)}{4\pi r_0 (1+M)}\,. \tag{21}$$

Since both sound fields p' of Eq. 19 and Eq. 21 must be equal, $\tilde{s}_{\mathrm{CAA}}$ and s_{CAA} are related by

$$\frac{\tilde{s}_{\mathrm{CAA}}(\tau_0^+)}{r_0} = \sum_m \mathrm{e}^{-(y_m - y_0)^2 \mu^{-2}} \frac{\partial_{\tau^+} s_{\mathrm{CAA}}(\tau_m^+)}{r_m}\,. \tag{22}$$

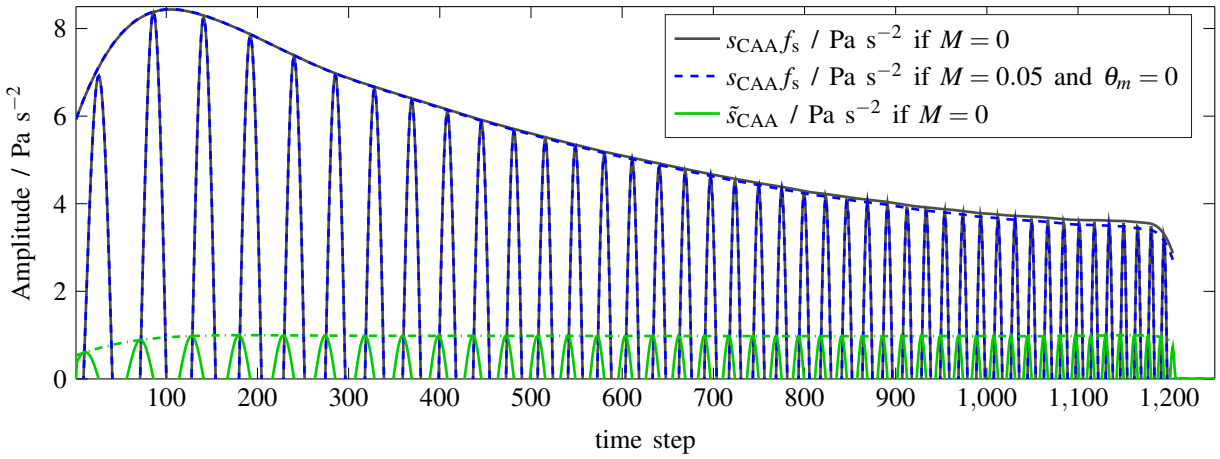

Figure 2. Two different types of source terms s_{CAA} and $\tilde{s}_{\mathrm{CAA}}$ corresponding to the same exponential sine sweep used as input signal throughout this work. While varying amplitude and phase this input signal is used for all loudspeakers. For better visibility, only the upper half of the signal is shown. Furthermore, the peak envelope for each signal is depicted, to highlight the different maximal amplitudes.

Thus, after converting s_{CAA} to $\tilde{s}_{\mathrm{CAA}}$ according to Eq. 22, $\tilde{s}_{\mathrm{CAA}}$ and $\tilde{s}_{\mathrm{CDPS}}$ are comparable.

For the present case without flow ($M = 0$) Fig. 2 shows the utilized exponential sine sweep, i.e., $\tilde{s}_{\mathrm{CAA}} \sim \sin(\omega_0 \mathrm{e}^{\alpha t} t)$. α determines the exponent of the frequency increase over time. Besides an initial and final fade out its amplitude is constant. The corresponding s_{CAA} signal – perfectly related by Eq. 22 – is also shown in Fig. 2.

The outer time derivative of a cos sweep gives a sine sweep (and vice versa), which explains the phase shift of $\pi/2$ between s_{CAA} and $\tilde{s}_{\mathrm{CAA}}$. The inner time derivative of the exponential frequency dependency of the sweep corresponds to the envelope curvature. In the case of homogeneous background flow with $M c_0 = 17.15\,\mathrm{m/s}$, the time delay between the different monopoles of the Gaussian distribution is either increased or reduced depending on the observer position (θ_m). However, this effect is restricted to high-frequency components (Fig. 2) and is negligible ($\pm 0.1\,\mathrm{dB}$) within the accuracy of the SPL errors discussed below. By increasing the ratio between the Gauss variance and the shortest wavelength, this flow effect completely disappears.

Once Eq. 22 is evaluated for a given signal (here a sine sweep), the conversion factor is universal for all speakers if – like in the present case – only the absolute phase and overall amplitude of the speaker signals differ. Thus, also the spectral ratio $\mathscr{F}[\tilde{s}_{\mathrm{CAA}}](f)/\mathscr{F}[s_{\mathrm{CAA}}](f)$ needs to be determined only once. Therein, $\mathscr{F}$ is the discrete Fourier transformation. Throughout the following spectral evaluation, this ratio will be applied to convert $s_{\mathrm{CAA}}(f)$ to $\tilde{s}_{\mathrm{CAA}}(f)$.

4.2 Spectral comparison of the original excitation signal and the adjoint-based solution

Fig. 3 depicts the gains of $\tilde{s}_{\mathrm{CAA}}$ provided by the CAA solver. Due to the used exponential sweep (cf. Fig. 2), higher frequencies have smaller time shares reflected by a decaying gain with increasing frequency in Fig. 3. The overall amplitude variation between the speakers causes the frequency independent offset.

Fig. 4 shows the phases of $\tilde{s}_{\mathrm{CAA}}$, featuring periodic 2π shifts as expected.

Fig. 5 and Fig. 6 show the gain and the phase differences between $\tilde{s}_{\mathrm{CDPS}}$ (reference solution of the CDPS model) and $\tilde{s}_{\mathrm{CAA}}$ (adjoint CAA solution). The maximal gain deviation error at the frequency interval edges is $\pm 0.25\,\mathrm{dB}$, and less than $\pm 0.15\,\mathrm{dB}$ between 1.5 kHz and 2.4 kHz for all speakers (Fig. 5). Hence, also the relative pressure levels between all five speakers are correctly captured. The phase deviation between the CAA

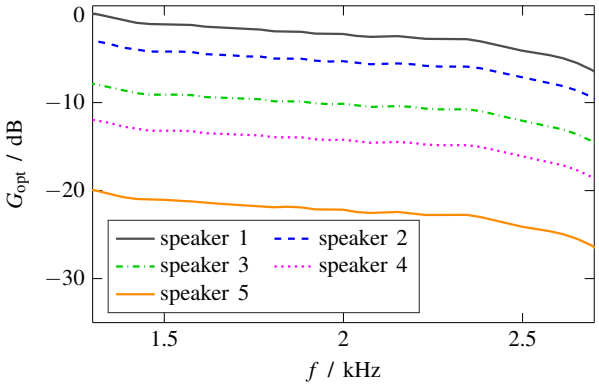

Figure 3. CAA solution of the input gains for all speakers. The SPL is normalized to the loudest speaker.

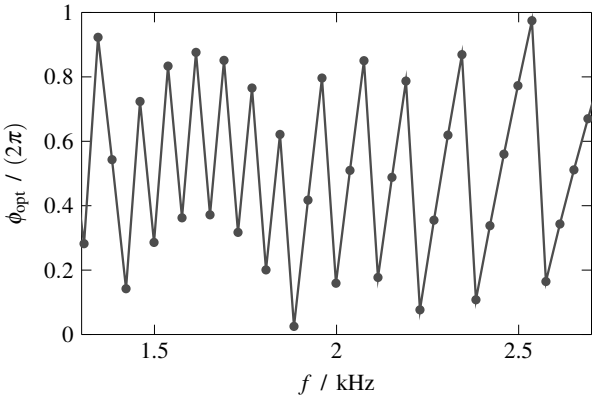

Figure 4. CAA solution of the input phase of the loudest speaker. All other speakers show qualitatively similar behavior.

and the CDPS solution corresponds to a phase shift of less than half a percent (phase shift in rad$/2\pi$) within the whole frequency interval (Fig. 6). Probably, the phase error is so small since a phase shift of p' in Eq. 5 has a greater impact on the objective in contrast to a perturbation of the pressure magnitude.

To conclude, the adjoint-based CAA solver is able to provide driving functions for the line array, which are comparable to the CDPS reference up to $\pm 0.25\,\mathrm{dB}$ and a phase error of half a percent.

5 SUMMARY

An adjoint-based framework for the determination of optimal driving functions of monopole speakers for sound reinforcement applications is presented. The effects of the employed Gaussian monopole implementation is discussed in detail. The required conversion function is derived analytically based on the analytic solution of the inhomogeneous wave equation including background flow. In summary, it has been shown that the approach is able to determine optimal driving functions, i.e., gain and delay, for a representative line array arrangement.

ACKNOWLEDGEMENTS

We acknowledge the financial support by the Deutsche Forschungsgemeinschaft (DFG) within the projects LE 3888/2-1 and WE 4057/16-1.

REFERENCES

[1] D. G. Meyer, “Computer simulation of loudspeaker directivity,” *J. Audio Eng. Soc.*, vol. 32, pp. 294–315, May 1984.

[2] G. W. J. van Beuningen and E. W. Start, “Optimizing directivity properties of DSP controlled loudspeaker arrays,” *Proc. of the Inst. of Acoustics: Reproduced Sound*, vol. 22, no. 6, pp. 17–37, 2000.

[3] P. Meyer and R. Schwenke, “Comparison of the directional point source model and BEM model for arrayed loudspeakers,” *Proc. of the Institute of Acoustics*, vol. 25, no. 4, 2003.

[4] S. Feistel, A. Thompson, and W. Ahnert, “Methods and limitations of line source simulation,” *J. Audio Eng. Soc.*, vol. 57, pp. 379–402, June 2009.

[5] L. Stein, F. Straube, J. Sesterhenn, S. Weinzierl, and M. Lemke, "Adjoint-based optimization of sound reinforcement including non-uniform flow," *submitted to The Journal of the Acoustical Society of America*, 2019.

[6] M. Giles and N. Pierce, "An introduction to the adjoint approach to design," *Flow, Turbulence and Combustion*, vol. 65, pp. 393–415, 2000.

[7] M. Lemke, *Adjoint based data assimilation in compressible flows with application to pressure determination from PIV data*. PhD thesis, Technische Universität Berlin, 2015.

[8] M. Lemke and J. Sesterhenn, "Adjoint-based pressure determination from PIV data in compressible flows – validation and assessment based on synthetic data," *European Journal of Mechanics - B Fluids*, vol. 58, pp. 29–38, 2016.

[9] M. Lemke, F. Straube, F. Schultz, J. Sesterhenn, and S. Weinzierl, "Adjoint-based time domain sound reinforcement," in *Audio Engineering Society Conference: 2017 AES International Conference on Sound Reinforcement – Open Air Venues*, Aug 2017.

[10] L. Stein, *Simulation and Modeling of a Helmholtz Resonator under Grazing Turbulent Flow*. PhD thesis, Technische Universität Berlin, 2019.

[11] F. Straube, F. Schultz, D. Bonillo, and S. Weinzerl, "An Analytical Approach for Optimizing the Curving of Line Source Arrays," *Journal of the Audio Engineering Society*, vol. 66, pp. 4–20, Feb. 2018.

[12] J. Delfs, "Basics of aeroacoustics," in *lecture notes, TU Braunschweig*, 2018.

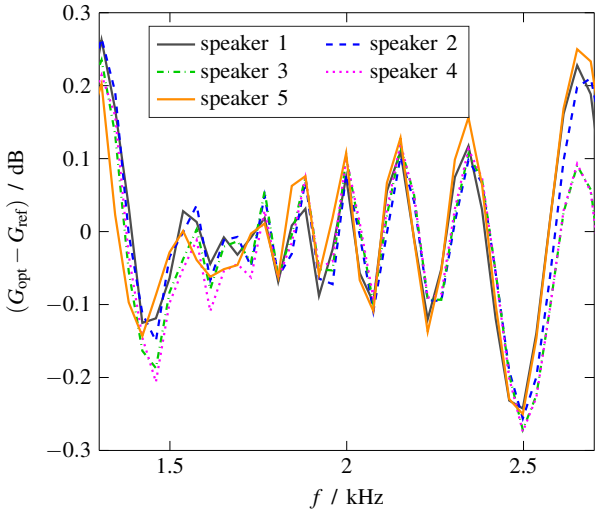

Figure 5. Difference between the CAA and the CDPS input gains of the speakers.

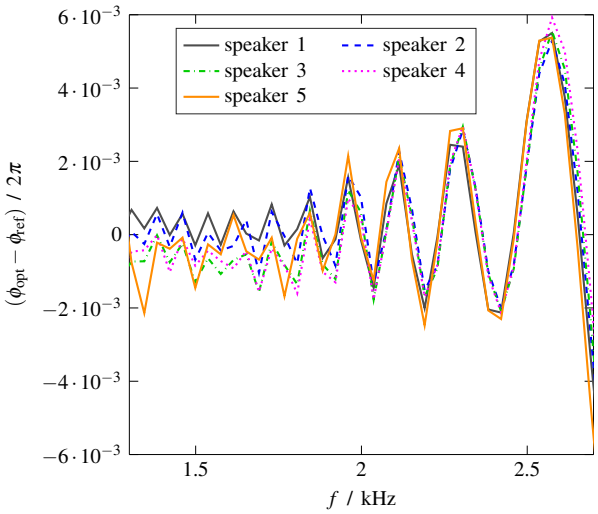

Figure 6. Difference between the CAA and the CDPS input phases of the speakers.